Applied Thermal Engineering 219 (2023) 119565

Contents lists available at ScienceDirect

Applied Thermal Engineering

journal homepage: www.elsevier.com/locate/apthermeng

Research Paper

Impacts of non-adsorbable gas on the adsorption-based desalination and cooling system with fin branch configurations

Mingliang Li, Yanan Zhao, Rui Long *, Zhichun Liu, Wei Liu

School of Energy and Power Engineering, Huazhong University of Science and Technology, Wuhan 430074, PR China

ARTICLE INFO

Keywords:
Adsorption desalination
Non-adsorbable gas
Fin branch
Machine learning

ABSTRACT

Non-adsorbable gas can significantly deteriorate the adsorption dynamics of the adsorption-based desalination and cooling system. In this study, an alternative complete computational fluid dynamic model involving non-adsorbable gas transportation is established. The impacts of non-adsorbable air originating from the incomplete degassing or leakage in the evaporator on the heat and mass transfer characteristics in the adsorbent bed and the performance of the adsorption-based desalination and cooling system are analyzed. Non-adsorbable air can significantly hinder the system performance due to weakened adsorption dynamics and induced additional mass transfer resistance. Moreover, a finned-tube bed attached with branched fins is employed to improve the heat transfer and adsorption dynamics. The impacts of fin configurations on the system performance with non-adsorbable air considered are systematically investigated. Machine learning is employed to construct the quantitative relationship between the fin configuration parameters and the total system throughput. And the optimal fin configuration is further identified via the genetic algorithm. The optimal fin configuration with the fin number of 12 and fin branch angle of 64.4° renders a 24.6% augmentation in the total cooling power and a 20.4% increase in total daily water production, respectively.

1. Introduction

The demand for potable water all over the world presents an exponential increase induced by the explosive development of population, agriculture, industry, and domestic applications. However, freshwater resources only account for 3 % of the natural water on the earth, most of the remaining is seawater. Desalination of brackish water or seawater paves promising ways to deal with the water shortage, especially for the people living in the Middle East or North Africa, suffering from semi-arid climate and extreme scarcity of freshwater. Adsorption-based desalination and cooling (ADC) technology is an environmentally friendly, cost-effective, and sustainable alternative to energy-intensive desalination [1–3]. In the ADC system, the thermal-driving adsorption-evaporation process via the hydrophilic solid particles such as silica gel, zeolite, and activated carbon exits [4,5]. The system presents advantages such as few moving parts and free of vibration [6–8]. The ADC system produces potable water through a desorption-condensation process when various types of low-grade renewable heat such as waste industrial heat [9], geothermal and solar energy [10,11] are supplied for the regeneration of water vapor which then liquesces in the condenser and transforms to freshwater [12].

However, the low system throughput and bulk volume due to the large heat and mass transfer resistance in the porous media become the fundamental obstacle to the commercialization of ADC technology [13–15]. Reasonable design of the adsorption heat exchanger can enhance the heat transfer process and elevate the system production, many researchers have carried out a detailed investigation on the structure of the adsorber [16,17]. Mitra et al. [18] established a two-dimensional computational fluid dynamic (CFD) transient model to examine the effects of particle diameter and heat exchanger aspect ratio on the adsorption dynamics in a rectangular bed. Results revealed that the bed with a smaller particle size shows a strong dependency on the flow resistance while weak dependency on the heat transfer and intra-particle resistance is observed for the larger particle size. Ilis et al. [19] conducted a numerical study on an annular bed with radial fins, the conduction heat transfer equation was non-dimensionalized to reduce the governing parameters to four, which was subsequently examined in detail. The results illustrated that heat transfer inside the adsorber can be improved by the fin only if the thermal diffusivity ratio and fin coefficient are low. Niazmand et al. [20] explored the effects of fin configurations including fin spacing, bed height and particle size on the

* Corresponding author.
E-mail address: r_long@hust.edu.cn (R. Long).

https://doi.org/10.1016/j.applthermaleng.2022.119565
Received 18 June 2022; Received in revised form 19 September 2022; Accepted 23 October 2022
Available online 28 October 2022

Nomenclature

C_p	Specific heat J kg^{-1} K^{-1}
COP	Coefficient of performance -
d_p	Particle diameter m
D_s	Mass diffusivity m^2/s
D_{so}	Pre-exponential factor m^2/s
E	Characteristic energy J/mol
E_a	Activation energy J/mol
H	Heat of adsorption J kg^{-1}
h_{fg}	Latent heat of vaporization J kg^{-1}
h	Convective heat transfer coefficient W/m^{-2}(−|-) K^{-1}
K	Permeability m^2
k	Thermal conductivity W/m K^{-1}
M	Mass kg
n	Surface heterogeneity factor -
P	Pressure Pa
q	Water uptake kg kg^{-1}
q_∞	Maximum adsorbent capacity kg kg^{-1}
q_o	Equilibrium uptake kg kg^{-1}
Q	Heat J
R	Universal gas constant J/mol K^{-1}
SCP	Specific cooling power kW kg^{-1}
SDWP	Specific daily water production m^3/ton day^{-1}
T	Temperature K
TCP	Total cooling power kW
TDWP	Total daily water production m^3/day
t	Time s
$\vec{U}$	Velocity vector m/s

Greek Symbols

ε	Porosity -
μ	Dynamic viscosity Pa s
ρ	Density kg m^{-3}
α	Thermal diffusivity, m^2/s

Subscripts

a	Air
ad	Adsorption
b	Bed
c	Cooling
con	Condenser
cw	Cooling water
cycle	Cycle time
des	Desorption
eva	Evaporation
eff	Effective
e	Evaporator
f	Fluid
g	Gas
h	Heating
ini	Initial
p	Particle
s	Saturation, solid
sg	Silica gel
t	Total
v	Vapor phase
w	Water

system performance via a transient two-dimensional CFD model in a cylindrical bed with annular fins. They observed that the total system production can be dramatically elevated at the cost of a slightly lower coefficient of performance. Subsequently, they investigated the bed configurations in a finned flat-tube adsorber and provided guidance on the design of this type of heat exchanger when it is dedicatedly used for adsorption systems, advancing an effective design procedure [21]. Saleh et al. [22] numerically and experimentally compared the performance of the wire finned, rectangular finned, and microchannel heat exchangers. Results revealed that the wire finned bed with aluminum fumarate [23] metal–organic framework (MOF) [24–26] shows superior performance in the water uptake. Li et al. [27] carried out a comprehensive investigation on the effects of bed porosity distribution and working conditions on the production and efficiency of a finned-tube cylindrical bed. An optimized scheme of bed porosity distribution was proposed, which presents a 16.2 % improvement over the uniform bed. Their other work involved a metal foam-packed annular bed, in which the foam and bed porosity are examined along with optimization of cycle control conditions [28]. They found that the system with a metal porosity of 0.8 and a bed porosity of 0.25 exhibits the best performance and the proposed cycle condition leads to an 11 % improvement in system throughput. Albaik et al. [29] investigated the performance of a wire-finned bed with aluminum fumarate integrated using coating and packing. The results presented that the coated adsorber outperforms the other two conditions in terms of cooling and water production.

In practice, the evacuated system may suffer from the extra mass transfer resistance from the non-adsorbable gas, consisting of the air due to leakage or desorption and hydrogen due to corrosion. Glaznev et al. [30] experimentally explored the effect of residual air on water adsorption, which presents a dramatic deterioration of system performance. The slowdown of adsorption may be attributed to the accumulation of non-adsorbable air in the particle surface as a gas-rich layer, which conduces extra resistance to the diffusion of this layer, as depicted in Fig. 1. However, the existing macrocosmic CFD model cannot capture the extremely complex adsorbent surface, the impact of non-adsorbable gas on the heat and mass transfer characteristics in the bed is examined via a model involving the diffusion equation for binary gas components.

Although the impact of residual air on the system performance is experimentally investigated, the underlying mechanisms and the heat and mass transfer characteristics in a bed with residual air lack further exploration. In order to reveal the impacts of non-adsorbable gas on the performance of adsorption-based desalination and cooling system and the underlying mechanisms, in this study, an alternative complete computational fluid dynamic model involving non-adsorbable gas transportation is established. The impacts of non-adsorbable air originating from the incomplete degassing or leakage in the evaporator on the heat and mass transfer characteristics in the adsorbent bed and the performance of the adsorption-based desalination and cooling system are analyzed. Moreover, a finned-tube bed with branched fins is employed to improve the heat transfer and adsorption dynamics. The impacts of fin numbers and fin branch angle on the system performance with non-adsorbable air included are systematically investigated. Machine learning is employed to construct the quantitative relationship between the fin configuration parameters and the total system throughput, and the optimal fin configuration is further revealed via the genetic algorithm.

2. Mathematical modeling

As presented in Fig. 2, the ADC system involves a finned-tube bed where the cold or hot water flows inside the tube with adsorbent particles filled outer the wall. Rectangular branched fins are installed in the bed to accelerate the heat and mass transfer dynamical characteristics. The tube is assumed with a length of 560 mm and the number of tubes is 40. The tube inner diameter R_0 and bed height H are fixed at 13 mm and 12 mm, while the tube thickness is 1 mm. As the bed length is much

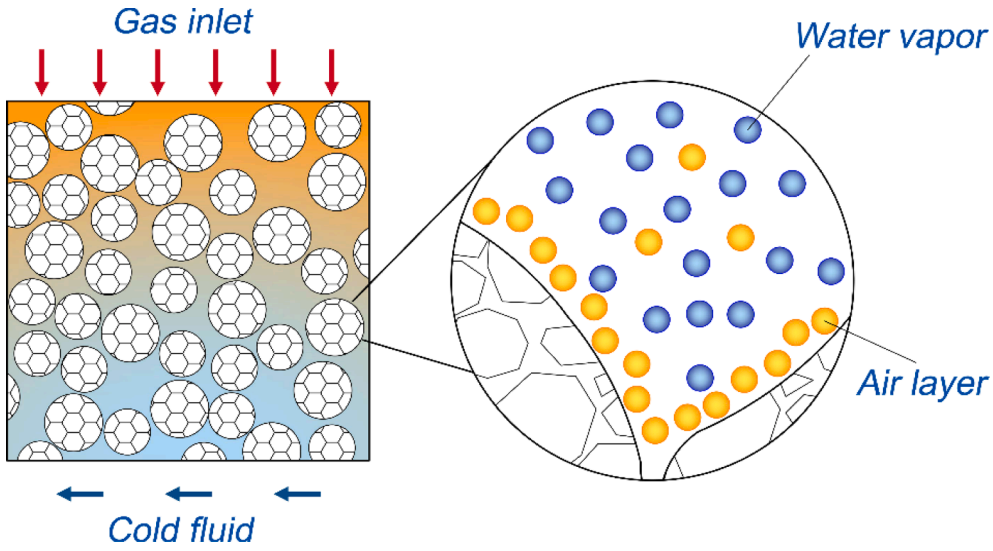

Fig. 1. Mass diffusion resistance induced by the residual air.

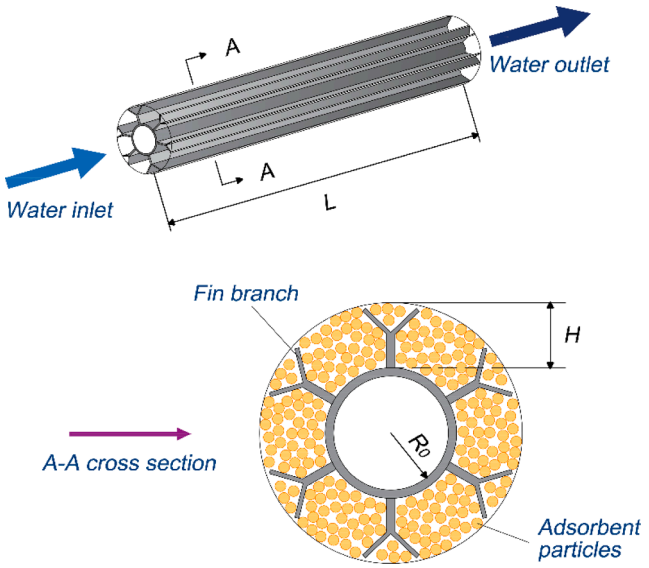

Fig. 2. Schematic diagram of the physical model.

larger than the radius, only the cross-section is chosen as the calculation domain, thus reducing the computational cost.

The model is established based on the following assumptions and simplifications [31]:

1. The adsorbent particles can be regarded as an ideal sphere with a constant diameter.
2. The mixed composition satisfies the gas equation of state, while the adsorbed water is a liquid phase.
3. The temperature and pressure of the evaporator and condenser are invariant, the variation of physical quantity along the tube and the effects of buoyancy can be neglected [21].
4. Pressure drop can be captured via Darcy's law, the bed satisfies the local thermal equilibrium assumption.
5. The convective heat transfer coefficient [32] and cold/hot water temperature are independent of time.
6. The impact of competitive adsorption and the microcosmic mechanism involving the adsorbent surface on the adsorption rate [33,34] is extremely complex, thus in the study adsorption of air by the adsorbent grains and the aforementioned effect are ignored.

2.1. Governing equations

The gas mixture consists of water vapor and non-adsorbable air. In the adsorbent bed, the mass conservation equation is solved by considering both diffusion and convection of each species [35–37]:

$$\frac{\partial y_i}{\partial t} + \vec{U}\cdot\nabla y_i + \rho_b \frac{RT}{P}\frac{(1-\varepsilon_b)}{\varepsilon_b}\frac{\partial q_i}{\partial t} - \nabla\cdot(D_a \nabla y_i) = 0, i = a, w \tag{1}$$

where y_i is the mole fraction of component i in the mixed gas. U is the gas velocity. ρ_b is the bed density. R is the universal gas constant. T is the bed temperature. P is the bed pressure. ε_b is the bed porosity. q is the uptake of component i. D_a is the gas diffusivity. components a and w represent air and water vapor, respectively. It should be emphasized that in the study, the adsorption of air by the adsorbent particles is neglected, thus the third term of the equation is 0 for the air.

The energy conversion equation in the adsorbent is [38]:

$$\begin{aligned}&(\varepsilon_b \rho_g C_{pg} + \rho_b (C_{ps} + qC_{pw}))\frac{\partial T}{\partial t}\\ &+\rho_g C_{pg}\vec{U}\cdot\nabla T = \nabla\cdot(k_{eff}\nabla T) + \rho_b \Delta H \frac{\partial q}{\partial t}\end{aligned} \tag{2}$$

where ρ_g is the gas density. C_{pg}, C_{ps}, and C_{pw} are the isobaric heat capacity of the gas phase, solid, and water, respectively. k_{eff} is the effective heat conductivity. ΔH is the adsorption heat of water vapor.

The heat transfer through the tube and fins is governed by [39,40]:

$$\frac{\partial T}{\partial t} = \alpha \nabla^2 T \tag{3}$$

where α is the thermal diffusivity of aluminum.

The adsorption dynamics is described by the linear driving force (LDF) model:

$$\frac{\partial q}{\partial t} = \frac{K_0 D_s}{d_p^2}(q_o - q) \tag{4}$$

where K_0 is the LDF constant with a unit of 1, D_s the surface diffusivity. d_p is the particle diameter. q_o is the equilibrium uptake of water vapor. The surface diffusivity D_s can be captured via the following equation:

$$D_s = D_{so}\exp(-\frac{E_a}{RT}) \tag{5}$$

where D_{so} is the pre-exponential factor. E_a is the activation energy.

The equilibrium uptake q_o is calculated through the D-A equation:

$$q_o = q_\infty \exp(-(\frac{RT}{E}\ln(\frac{p_s}{p}))^n) \quad (6)$$

where q_∞ is the maximum uptake of water vapor. E is the characteristic energy. p_s is the saturated pressure at bed temperature. p is the partial pressure of water vapor. n is the heterogeneity factor. Here, silica gel is employed as the adsorbent, whose dynamic and thermophysical characteristics are presented in Table 1.

As the gas velocity inside the bed is extremely low, the pressure drop is characterized by Darcy's law:

$$\overrightarrow{U} = -\frac{K}{\mu}\nabla P \quad (7)$$

where μ is the gas viscosity. K is the bed permeability which can be calculated via the Blake-Kozeny equation:

$$K = \frac{d_p^2 \varepsilon_b^3}{150(1-\varepsilon_b)^2} \quad (8)$$

The detailed simulation process is presented in Fig. 3. The performance of the ADC system is measured via the specific cooling power (SCP), the specific daily water production (SDWP), the total cooling power (TCP), the total daily water production (TDWP), the coefficient of performance (COP):

$$SCP = \frac{h_{fg}\Delta q_{av,ad}}{t_{cycle}}, TCP = M_s\frac{h_{fg}\Delta q_{av,ad}}{t_{cycle}} \quad (9)$$

$$SDWP = \frac{\Delta q_{av,des}}{\rho_w t_{cycle}}, TDWP = M_s\frac{\Delta q_{av,des}}{\rho_w t_{cycle}} \quad (10)$$

$$COP = \frac{Q_0}{Q_h} = M_s\frac{h_{fg}\Delta q_{av,ad}}{Q_{preh}+Q_{des}} \quad (11)$$

where h_{fg} is the latent heat of water vaporization. $\Delta q_{av,ad}$ and $\Delta q_{av,des}$ are the working capacity of adsorption and desorption. t_{cycle} is the cycle time. M_s is the adsorbent mass. ρ_w is the water density. Q_0 is the cooling power. Q_h is the total thermal energy demanded. Q_{preh} and Q_{des} are the heat input during preheating and desorption processes, respectively. The first two specific performance indicators consider the cooling and water production per unit adsorbent mass while the total performance indicators reflect the whole system throughput and the COP represents system refrigeration efficiency.

2.2. Boundary and initial conditions

The initial and boundary conditions employed in the simulation have been summarized in Table 2 and the boundary conditions during the adsorption-preheating-desorption-precooling phases are depicted in Fig. 4. The evaporator and condenser temperatures are fixed at 10℃ and 30℃, while the cooling and heating source are set at 30℃ and 85℃ with a constant convective heat transfer coefficient of 400 W/m^2 K. The initial temperature of the adsorbent bed is fixed at 60℃ and no residual air remains in the system. It should be noted that the non-adsorbable air assumed in the study originates from the incomplete degassing or leakage in the evaporator, thus the mixed composition flows into the bed during adsorption. The duration of adsorption and desorption are fixed at 500 s, while the preheating and precooling phase finish when the bed pressure reaches the condenser and evaporator pressure, as presented in Fig. 3. All the boundary and initial conditions are decided as an ordinary system driven by a low-grade heat source [43].

2.3. Grid independence

A finite element method in COMSOL Multiphysics 5.6 is employed to discretize the equations using backward difference approximation. The uptake is using a second-order discrete format while the temperature, pressure, velocity and gas fraction are discretized via a linear method. The triangular mesh is employed in the adsorbent part while the quadrilateral grid is used in the narrow fin domain, as shown in Fig. 4. The grid independence check is first conducted by monitoring the bed average temperature and uptake under various mesh element sizes. As presented in Fig. 5a, three different mesh sizes are examined (normal: 5120 elements; fine: 10,316 elements; finer: 37,436 elements). Results reveal that the deviation between average temperature under the selected three element sizes is rather slight. The grid convergence index (GCI) is calculated to estimate the accuracy induced by the mesh resolution. The expressions and defined quantities can be found in the literature [44]. The results indicate that the mesh convergence for temperature has a GCI of 0.0016 %. In order to reduce the computational cost, the normal-size mesh is employed in the simulation processes.

2.4. Model validation

As presented in Fig. 5b, the simulated transient average temperature and uptake are compared with the experimental results from [32], which involves a two-dimensional CFD study on the adsorption system using silica gel/water pair. In the simulation process, the air fraction is fixed at 0, while the initial bed temperature and pressure are set at 60℃ and 1228 Pa, respectively. The deviation between the calculated and experimental results is below 2 %, which demonstrates the accuracy of the model employed.

3. Results and discussion

As shown in Fig. 6, several complete ADC cycles are simulated thus to guarantee a stable output. The mole fraction is defined as the ratio of the amount of substance of air and the whole gas phase, which has a unit of 1. We can see that the system reaches the cyclic steady state after 4–5 cycles. The circulation starts with the adsorption phase where the water vapor is adsorbed and the bed is cooling. The non-adsorbable air flows into the bed, leading to a sudden water fraction drop. It should be emphasized that at the beginning of desorption, the water fraction tempestuously fluctuates due to the ephemeral adsorption induced by the sudden increase of the water vapor partial pressure, originating from the residual air in the adsorbent bed.

3.1. Impacts of the non-adsorbable gas

In this section, the impacts of the non-adsorbable gas on the dynamic heat and mass transfer processes are analyzed. Although in a practical system the mixing of air is relatively slight, the air fraction investigated in the study is fixed within a wide range (0–0.2) to amplify the effect of residual air on the heat and mass transfer characteristics and the system performance. In the calculation, the fin branch angle (Θ) is fixed at 65°, and the number of fins is 6, which induces a comparatively appropriate heat transfer enhancement while causing a slight impact on the mass transfer resistance. As shown in Fig. 7a and b, the average temperature of the adsorbent bed decreases, as adsorption heat released in the

Table 1
The thermophysical parameters of silica gel [41,42].

C_{ps} ($\frac{J.K}{kg}$)	E_a ($\frac{J}{mol.K}$)	D_{so} ($\frac{m^2}{s}$)	ρ_b ($\frac{kg}{m^3}$)	d_p (mm)	k_b ($\frac{W.K}{m}$)	$\triangle H$ ($\frac{kJ}{kg}$)	q_∞ ($\frac{kg_v}{kg_a}$)	E ($\frac{J}{mol}$)	n	K_0
924	42,000	2.54×10^{-4}	740	0.35	0.198	2415	0.37	4280	1.15	60

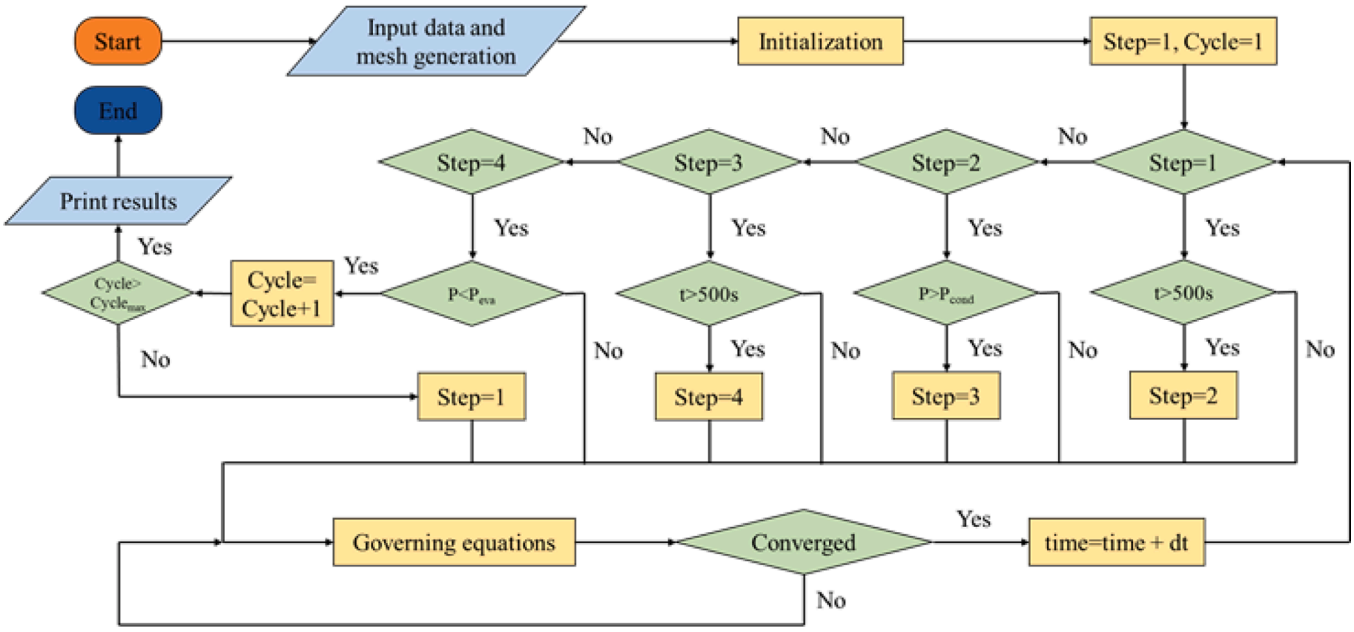

Fig. 3. Flow chart of the numerical simulation.

Table 2
Initial and boundary conditions.

Initial conditions	
$P_{ini} = P_{sat}@T_{eva}$; $T_{ini} = 60$℃; $q_{ini} = q_o(T_{ini}, P_{ini})$; $T_f(r = R_0) = T_{cw}$; $y_{a,ini} = 0$	
Boundary conditions	
$-k_{eff}\frac{\partial T}{\partial r}\|r = R_0 = h(T_f - T)$; $h = 400\ W/m^2\ K$; $T_{cw} = 30$℃; $T_{hw} = 85$℃; $T_{eva} = 10$℃; $T_{con} = 30$℃	
Adsorption	$T_f = T_{cw}$; $P(r = R) = P_{eva}$; $y_a(r = R) = 0$–0.2
Preheating	$T_f = T_{hw}$; $\frac{\partial P}{\partial r}\|r = R = 0$
Desorption	$T_f = T_{hw}$; $P(r = R) = P_{con}$
Precooling	$T_f = T_{cw}$; $\frac{\partial P}{\partial r}\|r = R = 0$

exothermic adsorption reaction is discharged by the cooling water flowing inside the tube. At the early stage of the adsorption process, the temperature of the adsorbent bed that has just finished the precooling remains at a relatively high level, which makes the bed still in a short ephemeral desorption state. The circulation of cold water rapidly decreases the temperature of adsorbent grains adjacent to the tube and fin surface where adsorption occurs.

The non-adsorbable air is mixed into the water vapor in the evaporator due to incomplete degassing or leakage. The presence of non-adsorbable air leads to a reduction of the partial pressure of water vapor that weakens the adsorption driving force. On the other hand, the non-adsorbable air arouses an extra mass transfer resistance to the inter and intra-particle resistance, which also is adverse to the adsorption dynamics. The above two reasons account for the reduction of adsorption uptake when non-adsorbable air is considered. The larger fraction of the non-adsorbable air, the lower the adsorption uptake. Meanwhile, the adsorption heat released is decreased, leading to lowered average bed temperature, as depicted in Fig. 7a.

As shown in Fig. 7c and d, due to the reduction of adsorption uptake, both SCP and SDWP present a negative relationship with the non-adsorbable air fraction. According to Eqs. (9) and (10), the total system production is governed by the working capacity and adsorbent mass. For the same fin configuration, the adsorbent mass is invariant when the air fraction increases, thus it can be observed from Fig. 8a and b that the total system performances (TCP and TDWP) both monotonically decrease with increasing non-adsorbable air fractions. For different fin configurations, the augmentation of the number of fins simultaneously impacts the heat transfer performance and the filled adsorbent mass, resulting in obvious improvement of both specific and total throughput. At larger fin numbers, the enhancement of heat transfer characteristics is more appealing compared with the reduction of adsorbent mass.

As shown in Fig. 8c, the presence of non-adsorbable air induces a deterioration of COP. According to Eq. (11), COP is defined as the ratio of generated cooling power and the consumed thermal energy via hot water circulation during preheating and desorption processes. Larger non-adsorbable air fraction leads to decreased water vapor uptake and lowered cooling power, which degrades the COP. Furthermore, heat and mass transfer improvement induced by inserting more fins into the bed leads to an obvious augment of the water vapor uptake and the COP.

3.2. Impacts of fin configurations

In this section, the impacts of fin configurations including the number of fins (N) and fin branch angle (Θ) on the ADC system performance are systematically analyzed. The number of fins is fixed within 3–10 while the fin branch angle is set at 0-85°, which is carefully considered to keep the adjacent fins from contacting. The non-adsorbable air fraction in the adsorption process is fixed at a constant value of 0.04, which is properly selected and close to reality.

3.2.1. Impacts of fin numbers

As shown in Fig. 9, the bed configuration with more fins exhibits a lower initial uptake and faster growth rate, which results in an intersection between different curves. More fins contribute to the heating and cooling processes. In the desorption process, large fin numbers augment the final temperature of the adsorbent bed, which contributes to desorption, therefore the initial uptake decreases with increasing fin numbers. Lower initial uptake is beneficial for adsorption. Therefore, at the early stage, due to enhanced adsorption, the adsorption heat under the fin configuration with a larger fin number is rather significant, leading to an elevated average temperature of the adsorbent bed. At the final stage of the adsorption process, the adsorption dynamic is relatively weakened, the cooling water could fast discharge the adsorption

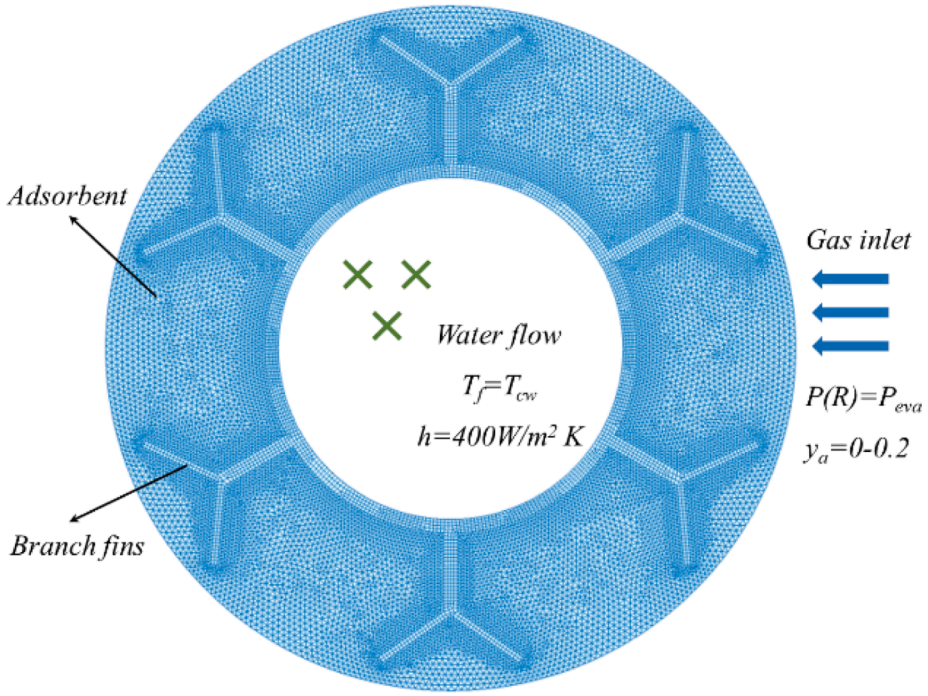

Fig. 4. Schematic of the mesh distribution and boundary conditions during the adsorption phase.

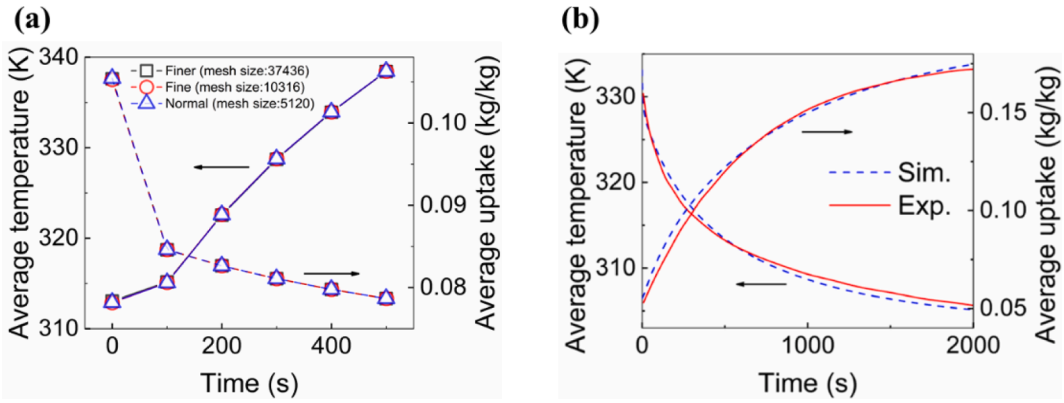

Fig. 5. (a) Impacts of mesh sizes on the temporal average temperature of the adsorbent bed; (b) comparisons of temporal average temperature and uptake between the simulation results and experimental data from Ref. [32].

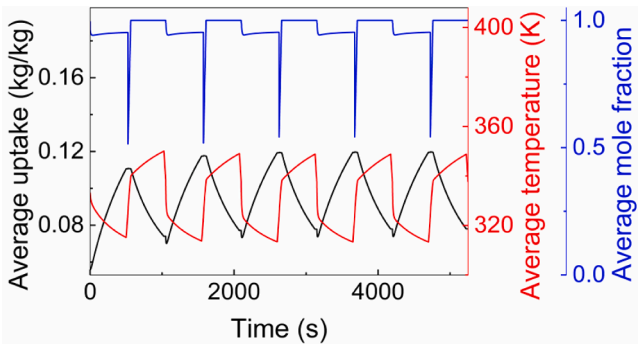

Fig. 6. Temporal histories of bed average temperature, average uptake, and average mole fraction of water from transient to cyclic steady state.

heat, which decreases the average temperature of the adsorbent, leading to augmented adsorption uptake, as shown in Fig. 9.

As shown in Fig. 9c, at the early stage, the water vapor fraction quickly drops due to the inflow of the outside non-adsorbable air. Meanwhile, the desiccative adsorbent grains adsorb the water intensely, and the percentage of water vapor in the bed rapidly falls to the minimum which is even smaller than the boundary fraction, then slightly increases due to weakened adsorption dynamics. Large fin numbers promote the adsorption process, lowering the water vapor fraction. It can be observed from Fig. 10a and b that the average bed temperature is lowered in the bed with more fins, contributing to the adsorption uptake in the regions comparatively far from the fin surface. The spatial distribution of air concentration is depicted in Fig. 10c. The air accumulating regions are concentrated in the area enclosed by the inner edge of the fin and the tube's outer wall, due to the drastic adsorption of the water vapor. Therefore, the augmentation of the number of fins induces a significant elevation of air concentration in the regions enclosed by the fins and the tube's outer wall.

The variations of specific and total performance indicators under

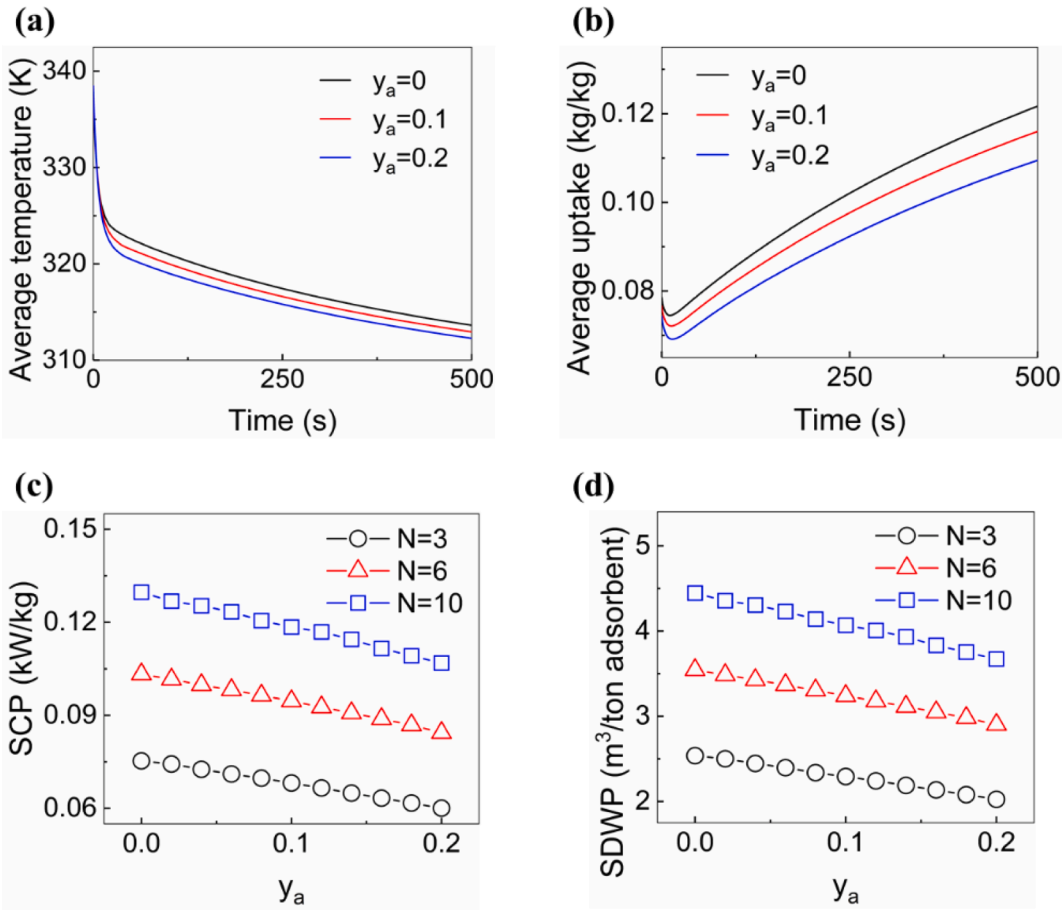

Fig. 7. Variations of (a) average temperature and (b) average uptake with adsorption time for different air fractions; variations of (c) SCP and (d) SDWP with the air fraction for different fin numbers.

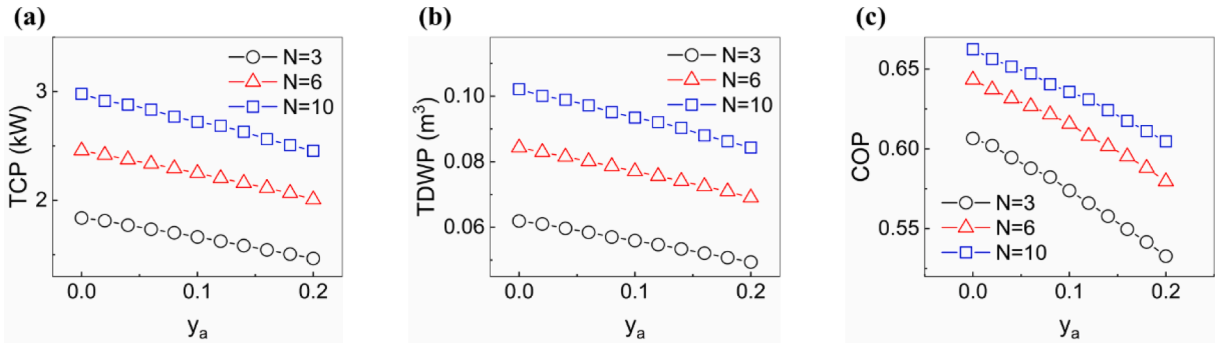

Fig. 8. Variations of (a) TCP, (b) TDWP, and (c) COP with the air fraction for different fin numbers.

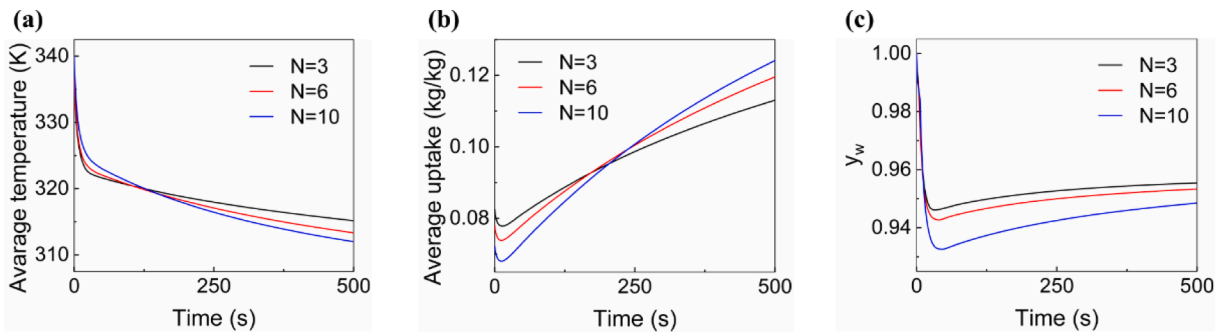

Fig. 9. Variations of (a) average temperature, (b) average uptake, and (c) average water fraction with adsorption time for different fin numbers.

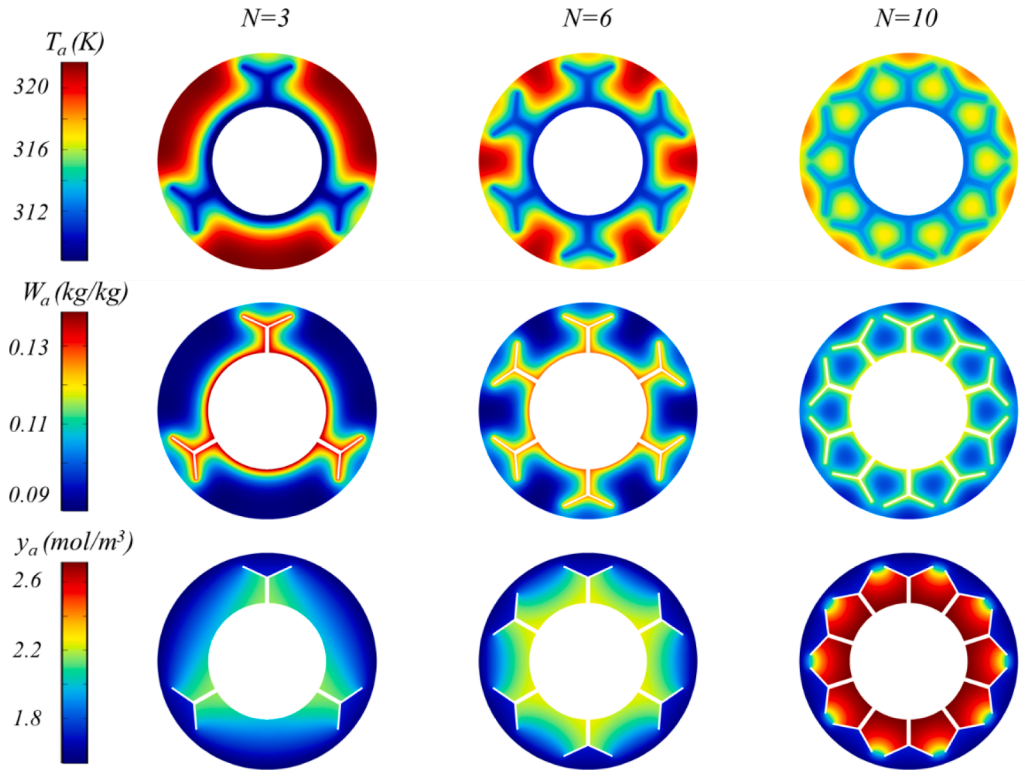

Fig. 10. (a) Temperature, (b) uptake, and (c) air concentration distributions with fin numbers of 3, 6, and 10 at 300 s of the isobaric adsorption process.

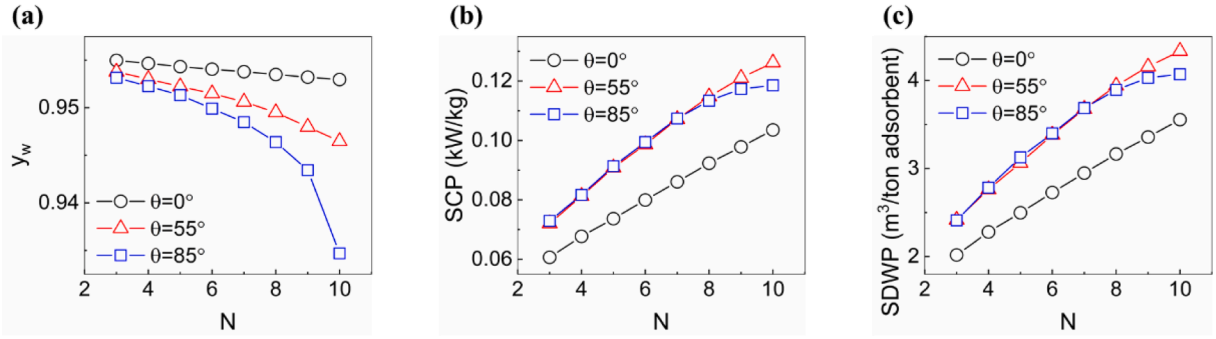

Fig. 11. Variations of (a) water fraction, (b) SCP, and (c) SDWP with the number of fins for different fin branch angles.

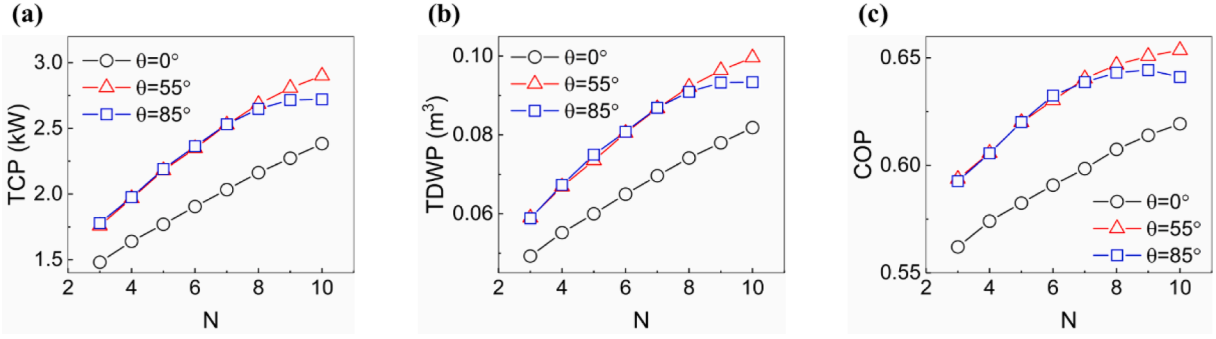

Fig. 12. Variations of (a) TCP, (b) TDWP, and (c) COP with the number of fins for different fin branch angles.

various fin numbers are depicted in Figs. 11 and 12. The presence of branch fins ($\Theta > 0°$) induces an elevation of system performance. For the fin configuration with 10 fins and no branches, an SCP of 0.104 kW/kg and an SDWP of 3.55 m^3/ton adsorbent per day are obtained. While the system with the same number of fins and a fin branch angle of 55° produces 0.126 kW/kg of cooling effect and 4.33 m^3/ton adsorbent of potable water per day, which are augmented by 21.9 %. However, as the fin branch angle is up to 85°, the system performance achieves barely

any improvement compared to that of 55°, which deteriorates at relatively more fins, as shown in Figs. 11 and 12. This discrepancy may originate from the reduction of water fraction with the larger number of fins and fin branch angle, which is caused by the extra enlarged mass diffusion resistance. The improvement of heat and mass transfer characteristics serves a more pronounced role than the reduction of adsorbent mass, resulting in upgraded total system production at large fin numbers, as shown in Fig. 12. The qualitative relationship between COP and fin configurations also presents the same phenomenon, due to the fact that both of them are basically governed by the working capacity. At a fin branch angle of 85°, there exists an optimal fin number ($N = 9$) leading to the highest COP of 0.644.

3.2.2. Impacts of fin branch angles

As shown in Fig. 13a, the average water fraction at 300 s of the adsorption phase under different fin branch angles and the number of fins are compared. More compact fin configurations (larger N and Θ) lead to the reduction of water vapor proportion, which arises from the more rapid water vapor adsorption and blocked gas diffusion by the attached branched fins. Augmenting the fin branch angle cannot always increase the working capacity. As shown in Figs. 13 and 14 that the system performance indicators increase with the fin branch angle augmenting, reach their maximum value then decrease. There exists an optimal fin branch angle. The system with ten fins and a fin branch angle of approximately 55° produces 0.126 kW/kg of cooling and 4.33 m^3/ton adsorbent of desalinated water per day, which presents a 21.9 % improvement of the bed with no branch fins. The system generates a TCP of 2.90 kW and TDWP of 0.0996 m^3 per day, exhibiting 21.7 % of elevation than the conventional system with no branch fins. The highest COP reaches 0.654, which is of 5.5 % improvement from the bed with no branch fins. As shown in Fig. 15, in general, two factors account for the phenomenon induced by the variation of fin branch angles: (i) the augmentation of the fin branch angle enhances the heat transfer in the adsorbent bed and the improvement becomes slight when the angle is large enough; (ii) the fin branch causes a dramatic increase of mass diffusion resistance. At small fin branch angles, a more pronounced improvement of the heat transfer performance decreases the bed temperature in the adsorption process and increases that in the desorption process, which contributes to the adsorption dynamics. At large fin branch angles, the fin branch hinders the water vapor passing in, which is adverse to adsorption. Furthermore, the optimal fin branch angle decreases due to the augmentation of the number of fins.

3.3. Machine learning and optimization

The effect of fin configuration on the total system production is furtherly examined in Fig. 17a and b, which clearly present the presence of optimal fin branch angle, especially for a larger number of fins. In order to obtain the optimal fin configurations, based on the numerical calculation results, an ensemble-based machine learning model is established to acquire the hidden quantitative relationship between fin configurations and TCP and TDWP. Machine learning is a mathematical tool using a specific algorithm to investigate the potential quantitative relationship between variables and labels. The main procedure is conducted in the regression learner module based on the Matlab platform. The detailed flow chart is presented in Fig. 16a, where the genetic algorithm is employed using trained models derived from the machine learning step to determine the optimal fin configuration.

The accuracy of the machine learning method is generally captured by the training error and generalization error. As the latter is difficult to decrease and needs specific designing of algorithm which is not the main object of the study, the random error is measured by applying four common statistics: Root mean square error (RMSE), R2, mean absolute error (MAE), and mean square error (MSE) to estimate the training error which are summarized in Table 3. The ensemble-based model utilized in the machine learning step is trained several times to reduce the training error. The training data is divided into five, four of which are used as the training set and the rest for the testing set, which is called the fivefold cross-validation. Furthermore, to validate the veracity of the model in predicting the system production of cooling and water, the predicted and simulated TCP and TDWP are, respectively, compared in Fig. 16b and c, which manifests the credibility of the trained models.

As presented in Fig. 17c and d, the increase of the number of fins and the reduction of air proportion simultaneously lead to the augmentation of the optimal cooling effect and water production. The system with 12 fins and a fin branch angle of 64.4° generates the optimal TCP of 2.91 kW, while the highest TDWP of 0.1015 m^3 per day is derived from the bed inserted with 12 fins with an angle of 64.2°. In a well-sealed system with no residual air, the optimal fin branch angle decreases as the number of fins increases. It should be noted that in a bed with 2 fins, the optimal fin branch angle reaches 90° (the upper bound set in the genetic algorithm), which illustrates that in these cases, the system throughput shows a monotonous trend with fin branch angle. However, when a certain percentage of air mixes into the system, the optimal fin branch angle varies irregularly with the number of fins, which may arise due to the compromise between the improved heat transfer characteristics and augmented diffusion resistance.

4. Conclusion

The study is dedicated to exploring the impact of non-adsorbable air on the heat and mass transfer characteristics inside the adsorption bed via an alternative complete computational fluid dynamic model along with the component transportation equation. The significant deterioration of cooling and water production induced by the residual air illustrated that aging pipes and leakage of air can be serious problems in the long time operation of a practical ADC system. Moreover, the tube-finned adsorbent bed is advanced with branched fins to improve the heat and mass transfer characteristics. The optimization of fin configuration is conducted under various air fractions employing machine learning and genetic algorithm. The elevation of system throughput reveals that the bed with branched fins performs better than that with

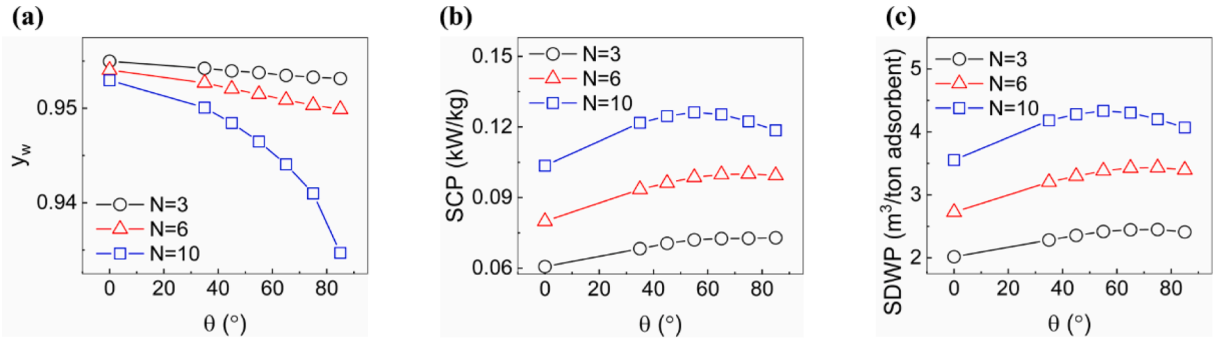

Fig. 13. Variations of (a) water fraction, (b) SCP, and (c) SDWP with the fin branch angle for different fin numbers.

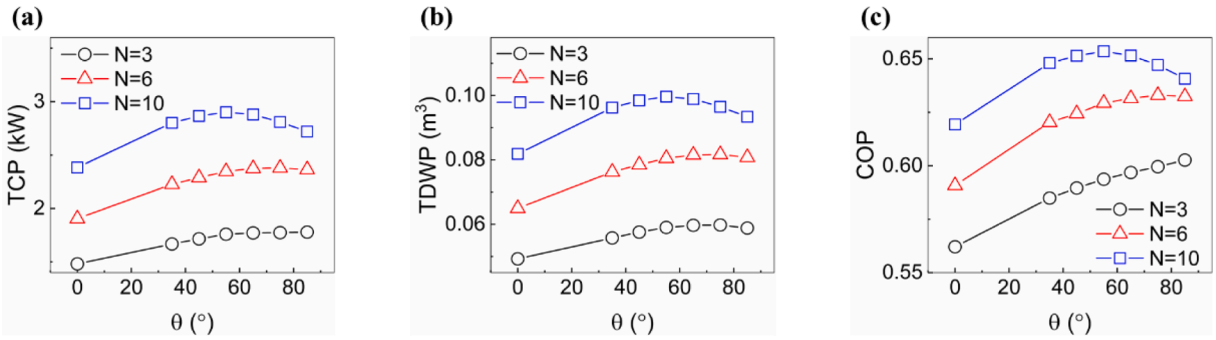

Fig. 14. Variations of (a) TCP, (b) TDWP, and (c) COP with the fin branch angle for different fin numbers.

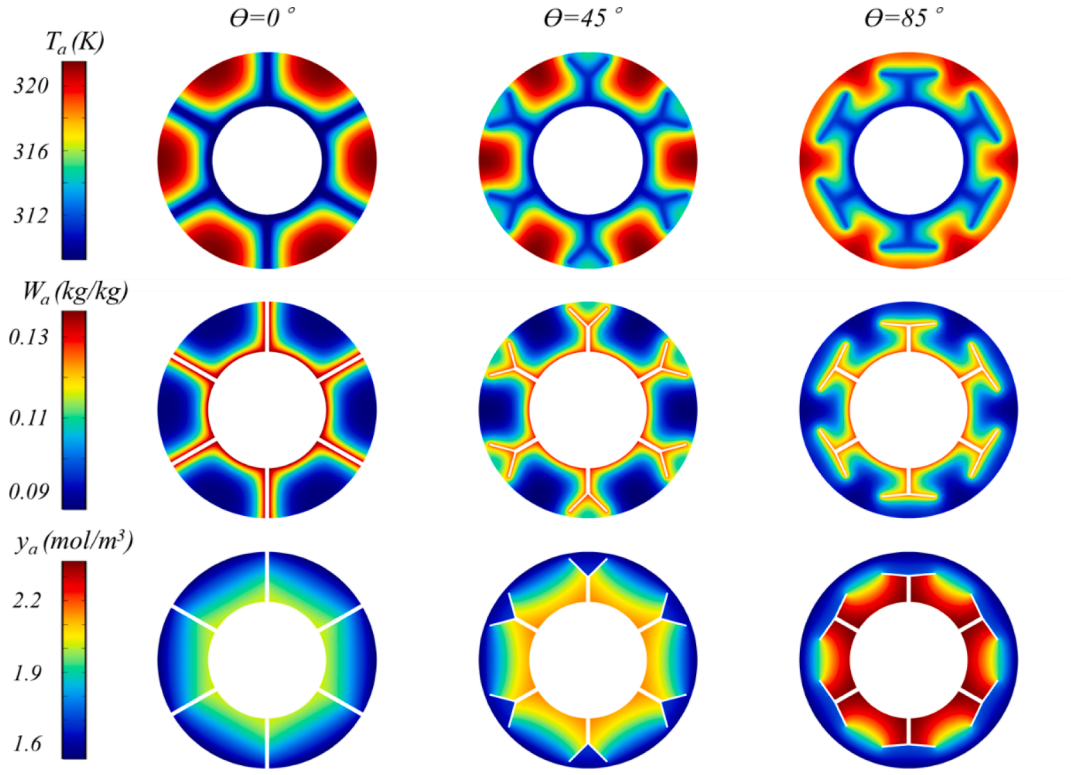

Fig. 15. (a) Temperature, (b) uptake, and (c) air concentration distributions with fin branch angles of 0°, 45°, and 85° at 300 s of the isobaric adsorption process.

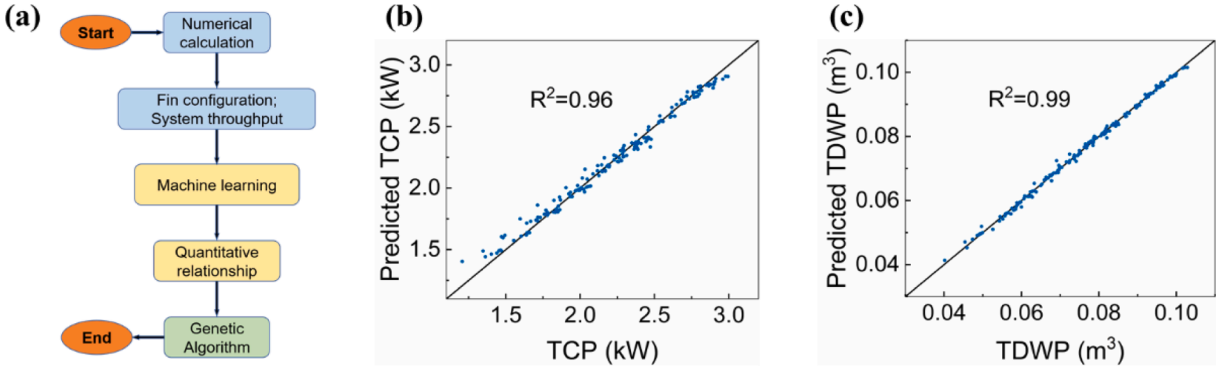

Fig. 16. (a) Flow chart for the machine learning procedure; comparisons between predicted and calculated (b) TCP and (c) TDWP during the ensemble-based machine learning process.

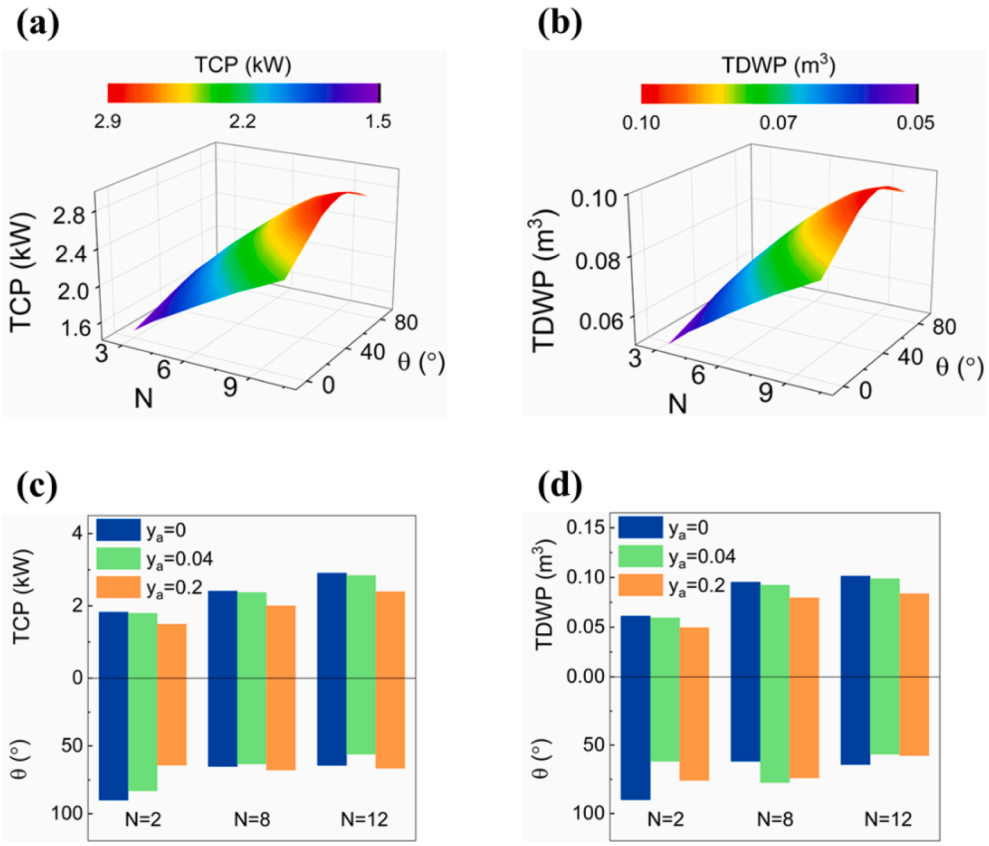

Fig. 17. Simulation points of (a) TCP and (b) TDWP for different fin numbers and fin branch angles at the air fraction of 0.04; comparisons of (c) TCP and (d) TDWP at optimal fin branch angles for different air fractions and the number of fins.

Table 3
Accuracy of the machine learning methods.

Trained factor	RSME	R^2	MSE	MAE
TCP	0.0080055	0.96	0.0064088	0.061695
TDWP	0.0016623	0.99	0.0000027632	0.0011389

rectangular fins, which serves as guidance in designing efficient adsorbent beds. General findings are listed below:

- Non-adsorbable air significantly hinders the system performance due to weakened adsorption dynamics and induced additional mass transfer resistance.
- The contradictory factors (the enhancement of heat transfer in the adsorbent bed and the increase of mass diffusion resistance) account for the optimal fin branch angle on cooling and water production.
- The quantitative relationship between the fin configuration parameters and the total system throughput is constructed via machine learning.
- The optimal fin configuration with the fin number of 12 and fin branch angle of 64.4° renders a 24.6 % augmentation in the total cooling power and a 20.4 % increase in total daily water production, respectively.

CRediT authorship contribution statement

Mingliang Li: Writing – original draft. **Yanan Zhao:** Visualization. **Rui Long:** Conceptualization, Writing – review & editing. **Zhichun Liu:** Investigation. **Wei Liu:** Formal analysis.

Declaration of Competing Interest

The authors declare that they have no known competing financial interests or personal relationships that could have appeared to influence the work reported in this paper.

Data availability

No data was used for the research described in the article.

Acknowledgments

This work was financially supported by the National Natural Science Foundation of China (52176070).

References

[1] S. Lin, H. Zhao, L. Zhu, T. He, S. Chen, C. Gao, et al., Seawater desalination technology and engineering in China: a review, Desalination 498 (2021).
[2] K.C. Ng, K. Thu, S.J. Oh, L. Ang, M.W. Shahzad, A.B. Ismail, Recent developments in thermally-driven seawater desalination: energy efficiency improvement by hybridization of the MED and AD cycles, Desalination 356 (2015) 255–270.
[3] M. Li, Y. Zhao, R. Long, Z. Liu, W. Liu, Field synergy analysis for heat and mass transfer characteristics in adsorption-based desalination and cooling systems, Desalination 517 (2021) 115244.
[4] M.F. Chairunnisa, T. Miyazaki, K. Thu, J. Miyawaki, K. Nakabayashi, et al., Theoretical dehumidification capacity of acorn nutshell-based activated carbon under two Asian urban cities' ambient air condition, Int. J. Refrig. 131 (2021) 137–145.
[5] M.F. Chairunnisa, T. Miyazaki, K. Thu, J. Miyawaki, K. Nakabayashi, et al., Enhancing water adsorption capacity of acorn nutshell based activated carbon for adsorption thermal energy storage application, Energy Rep. 6 (2020) 255–263.
[6] H. Zhang, H. Ma, S. Liu, H. Wang, Y. Sun, D. Qi, Investigation on the operating characteristics of a pilot-scale adsorption desalination system, Desalination 473 (2020) 114196.

[7] M. Ghazy, A.A. Askalany, K. Harby, M.S. Ahmed, Adsorption isotherms and kinetics of HFC-404A onto bituminous based granular activated carbon for storage and cooling applications, Appl. Therm. Eng. 105 (2016) 639–645.
[8] K. Thu, A. Chakraborty, Y.-D. Kim, A. Myat, B.B. Saha, K.C. Ng, Numerical simulation and performance investigation of an advanced adsorption desalination cycle, Desalination 308 (2013) 209–218.
[9] A.G. Olabi, K. Elsaid, M.K.H. Rabaia, A.A. Askalany, M.A. Abdelkareem, Waste heat-driven desalination systems: Perspective. Energy 209 (2020).
[10] A.S. Alsaman, A.A. Askalany, K. Harby, M.S. Ahmed, Performance evaluation of a solar-driven adsorption desalination-cooling system, Energy. 128 (2017) 196–207.
[11] C. Olkis, S. Al-Hasni, S. Brandani, S. Vasta, G. Santori, Solar powered adsorption desalination for Northern and Southern Europe, Energy. 232 (2021).
[12] J.W. Wu, M.J. Biggs, P. Pendleton, A. Badalyan, E.J. Hu, Experimental implementation and validation of thermodynamic cycles of adsorption-based desalination, Appl. Energy 98 (2012) 190–197.
[13] K. Thu, K.C. Ng, B.B. Saha, A. Chakraborty, S. Koyama, Operational strategy of adsorption desalination systems, Int. J. Heat Mass Transf. 52 (7–8) (2009) 1811–1816.
[14] S.-Y. Woo, H.-S. Lee, H. Ji, D.-S. Moon, Y.-D. Kim, Silica gel-based adsorption cooling cum desalination system: focus on brine salinity, operating pressure, and its effect on performance, Desalination 467 (2019) 136–146.
[15] M.M. Abd-Elhady, A.M. Hamed, Effect of fin design parameters on the performance of a two-bed adsorption chiller, Int. J. Refrig 113 (2020) 164–173.
[16] S. Mitra, N. Aswin, P. Dutta, Scaling analysis and numerical studies on water vapour adsorption in a columnar porous silica gel bed, Int. J. Heat Mass Transf. 95 (2016) 853–864.
[17] M. Mahdavikhah, H. Niazmand, Effects of plate finned heat exchanger parameters on the adsorption chiller performance, Appl. Therm. Eng. 50 (1) (2013) 939–949.
[18] S. Mitra, M. Muttakin, K. Thu, B.B. Saha, Study on the influence of adsorbent particle size and heat exchanger aspect ratio on dynamic adsorption characteristics, Appl. Therm. Eng. 133 (2018) 764–773.
[19] G.G. Ilis, M. Mobedi, S. Ülkü, A dimensionless analysis of heat and mass transport in an adsorber with thin fins; uniform pressure approach, Int. Commun. Heat Mass Transfer 38 (6) (2011) 790–797.
[20] H. Niazmand, I. Dabzadeh, Numerical simulation of heat and mass transfer in adsorbent beds with annular fins, Int. J. Refrig 35 (3) (2012) 581–593.
[21] M. Mohammadzadeh Kowsari, H. Niazmand, M.M. Tokarev, Bed configuration effects on the finned flat-tube adsorption heat exchanger performance: numerical modeling and experimental validation, Appl. Energy 213 (2018) 540–554.
[22] M.M. Saleh, R. Al-Dadah, S. Mahmoud, E. Elsayed, O. El-Samni, Wire fin heat exchanger using aluminium fumarate for adsorption heat pumps, Appl. Therm. Eng. 164 (2020) 114426.
[23] E. Elsayed, R. Al-Dadah, S. Mahmoud, P. Anderson, A. Elsayed, Experimental testing of aluminium fumarate MOF for adsorption desalination, Desalination 475 (2020).
[24] R. Al-Dadah, S. Mahmoud, E. Elsayed, P. Youssef, F. Al-Mousawi, Metal-organic framework materials for adsorption heat pumps, Energy. 190 (2020).
[25] H.J. Dakkama, P.G. Youssef, R.K. Al-Dadah, S. Mahmoud, Adsorption ice making and water desalination system using metal organic frameworks/water pair, Energy Convers. Manage. 142 (2017) 53–61.
[26] A. Askalany, A.S. Alsaman, M. Ghazy, R.H. Mohammed, R. Al-Dadah, S. Mahmoud, Experimental optimization of the cycle time and switching time of a metal organic framework adsorption desalination cycle, Energy Convers. Manage. 245 (2021) 114558.
[27] M. Li, Y. Zhao, R. Long, Z. Liu, W. Liu, Computational fluid dynamic study on adsorption-based desalination and cooling systems with stepwise porosity distribution, Desalination 508 (2021) 115048.
[28] M. Li, Y. Zhao, R. Long, Z. Liu, W. Liu, Metal foam packed adsorbent bed boosting the performance of the adsorption-based desalination and cooling system, Energy Convers. Manage. 254 (2022).
[29] I. Albaik, R. Al-Dadah, S. Mahmoud, M.A. Ismail, M.K. Almesfer, Coated, packed and combined wire finned tube adsorption cooling and desalination system using metal-organic framework: numerical study, Energy. 247 (2022).
[30] I.S. Glaznev, Y.I. Aristov, Kinetics of water adsorption on loose grains of SWS-1L under isobaric stages of adsorption heat pumps: the effect of residual air, Int. J. Heat Mass Transf. 51 (25–26) (2008) 5823–5827.
[31] J.W. Wu, M.J. Biggs, E.J. Hu, Dynamic model for the optimisation of adsorption-based desalination processes, Appl. Therm. Eng. 66 (1–2) (2014) 464–473.
[32] R.H. Mohammed, O. Mesalhy, M.L. Elsayed, L.C. Chow, Scaling analysis of heat and mass transfer processes in an adsorption packed bed, Int. J. Therm. Sci. 133 (2018) 82–89.
[33] E. Oktariani, K. Tahara, K. Nakashima, A. Noda, B. Xue, A.T. Wijayanta, et al., Experimental investigation on the adsorption process for steam generation using a zeolite-water system, J. Chem. Eng. Jpn. 45 (5) (2012) 355–362.
[34] B. Xue, K. Tahara, K. Nakashima, A. Noda, E. Oktariani, A.T. Wijayanta, et al., Numerical simulation for steam generation process in a novel zeolite-water adsorption heat pump, J. Chem. Eng. Jpn. 45 (6) (2012) 408–416.
[35] D. Cheng, E.A.J.F. Peters, J.A.M. Kuipers, Performance study of heat and mass transfer in an adsorption process by numerical simulation, Chem. Eng. Sci. 160 (2017) 335–345.
[36] F.N. Al-Mousawi, R. Al-Dadah, S. Mahmoud, Different bed configurations and time ratios: Performance analysis of low-grade heat driven adsorption system for cooling and electricity, Energy Convers. Manage. 148 (2017) 1028–1040.
[37] M.A. Makarem, M. Farsi, M.R. Rahimpour, CFD simulation of CO2 removal from hydrogen rich stream in a microchannel, Int. J. Hydrogen Energy 46 (37) (2021) 19749–19757.
[38] İ. Solmuş, S. Andrew, D. Rees, C. Yamalı, D. Baker, A two-energy equation model for dynamic heat and mass transfer in an adsorbent bed using silica gel/water pair, Int. J. Heat Mass Transf. 55 (19–20) (2012) 5275–5288.
[39] M.A. Aziz, I.A.M. Gad, E.S.F.A. Mohammed, R.H. Mohammed, Experimental and numerical study of influence of air ceiling diffusers on room air flow characteristics, Energy Build. 55 (2012) 738–746.
[40] R.H. Mohammed, A simplified method for modeling of round and square ceiling diffusers, Energy Build. 64 (2013) 473–482.
[41] K. Thu, A. Chakraborty, B.B. Saha, K.C. Ng, Thermo-physical properties of silica gel for adsorption desalination cycle, Appl. Therm. Eng. 50 (2) (2013) 1596–1602.
[42] R.H. Mohammed, O. Mesalhy, M.L. Elsayed, L.C. Chow, Performance evaluation of a new modular packed bed for adsorption cooling systems, Appl. Therm. Eng. 136 (2018) 293–300.
[43] S. Mitra, P. Kumar, K. Srinivasan, P. Dutta, Performance evaluation of a two-stage silica gel + water adsorption based cooling-cum-desalination system, Int. J. Refrig 58 (2015) 186–198.
[44] M. Sosnowski, Evaluation of heat transfer performance of a multi-disc sorption bed dedicated for adsorption cooling technology, Energies 12 (24) (2019).